av = 1.9 percent, |max| = 5.4 percent (at three points, for $W/\lambda_0 > 0.8$)

$$3.8 \leqslant \epsilon_r \leqslant 9.8$$

$$0.0015 \leqslant W/\lambda_0 \leqslant 0.075$$

$$\lambda'/\lambda_0 = 0.9217 - 0.277 \ln \epsilon_r + 0.0322(W/d)\left[\frac{\epsilon_r}{(W/d + 0.435)}\right]^{1/2} - 0.01 \ln(d/\lambda_0)\left[4.6 - \frac{3.65}{\epsilon_r^2 \sqrt{W/\lambda_0}\,(9.06 - 100 W/\lambda_0)}\right] \tag{12}$$

av = 0.6 percent, |max| = 3 percent (at three points, occurs for $W/d > 1$ and $\epsilon_r > 6.0$)

$$Z_0 = 73.6 - 2.15\epsilon_r + (638.9 - 31.37\epsilon_r)(W/\lambda_0)^{0.6} + \left(36.23\sqrt{\epsilon_r^2 + 41} - 225\right)\frac{W/d}{(W/d + 0.876\epsilon_r - 2)} + 0.51(\epsilon_r + 2.12)(W/d)\ln(100 d/\lambda_0) - 0.753\epsilon_r (d/\lambda_0)/\sqrt{W/\lambda_0} \tag{13}$$

av = 1.58 percent, max = 5.4 percent (at three points, occurs for $W/d > 1.67$)

$$0.075 \leqslant W/\lambda_0 \leqslant 1.0$$

$$\lambda'/\lambda_0 = 1.05 - 0.04\epsilon_r + 1.411 \times 10^{-2}(\epsilon_r - 1.421) \cdot \ln\{W/d - 2.012(1 - 0.146\epsilon_r)\} + 0.111(1 - 0.366\epsilon_r)\sqrt{W/\lambda_0} + 0.139(1 + 0.52\epsilon_r \ln(14.7 - \epsilon_r))(d/\lambda_0)\ln(d/\lambda_0) \tag{14}$$

av = 0.75 percent, |max| = 3.2 percent (at two points, occurs for $W/\lambda_0 = 0.075$, $d/\lambda_0 > 0.03$)

$$Z_0 = 120.75 - 3.74\epsilon_r + 50\left[\tan^{-1}(2\epsilon_r) - 0.8\right] \cdot (W/d)^{[1.11 + (0.132(\epsilon_r - 27.7)/(100 d/\lambda_0 + 5))]} \cdot \ln\left[100 d/\lambda_0 + \sqrt{(100 d/\lambda_0)^2 + 1}\right] + 14.21(1 - 0.458\epsilon_r)(100 d/\lambda_0 + 5.1 \ln \epsilon_r - 13.1) \cdot (W/\lambda_0 + 0.33)^2 \tag{15}$$

av = 2.0 percent, |max| = 5.8 percent (at two points, occurs for $W/\lambda_0 < 0.1$). In the above formula, $\tan^{-1}(\cdot)$ assumes its principal value.

III. Conclusion

A spectral-domain Galerkin method is used to compute the characteristic impedance of wide slotlines on low-ϵ_r substrates. Empirical formulas have been presented for the slot wavelength and the characteristic impedance over a wide range of slot widths. The data presented here supplement data already available on high-ϵ_r substrates.

References

[1] R. Janaswamy and D. H. Schaubert, "Dispersion characteristics for wide slotlines on low permittivity substrates," *IEEE Trans. Microwave Theory Tech.*, vol. MTT-33, pp. 723–726, Aug. 1985.

[2] J. B. Knorr and K. Kuchler, "Analysis of coupled slots and coplanar strips on dielectric substrate," *IEEE Trans. Microwave Theory Tech.*, vol. MTT-23, pp. 541–548, July 1975.

[3] E. A. Mariani *et al.*, "Slotline characteristics," *IEEE Trans. Microwave Theory Tech.*, vol. MTT-17, pp. 1091–1096, Dec. 1969.

[4] E. L. Kollberg *et al.*, "New results on tapered slot endfire antennas on dielectric substrate," presented at the 8th IEEE Int. Conf. Infrared, Millimeter Waves, Miami, FL, Dec. 1983.

[5] S. N. Prasad and S. Mahapatra, "A new MIC slot line, aerial," *IEEE Trans. Antennas Propagat.*, vol. AP-31, pp. 525–527, May 1983.

[6] J. F. Johansson, "Investigation of some slotline antennas," M.S. thesis, Chalmers University, Gothenberg, Sweden, 1983.

[7] T. Itoh and R. Mittra, "Dispersion characteristics of slot lines," *Electron. Lett.*, vol. 7, pp. 364–365, July 1971.

[8] A. Erdelyi *et al.*, *Tables of Integral Transforms*, vol. 2. New York: McGraw-Hill, 1954.

A Broad-Band Homodyne Network Analyzer with Binary Phase Modulation

UWE GÄRTNER, MEMBER, IEEE, AND
BURKHARD SCHIEK, MEMBER, IEEE

***Abstract*—An automatic homodyne network analyzer system using cascaded binary phase shifters is described which operates over the full *X*-band with a high dynamic range due to an auxiliary modulation and linear detection technique. A general analytic solution of the complex nonlinear system equations is given which allows the use of a coupled modulator/phase shifter structure. Measurement results are reported.**

Nomenclature

$\boldsymbol{B}_u, \boldsymbol{B}_l$	Modulator conversion losses for the first upper and lower sidebands.
$\tilde{\boldsymbol{B}}_u, \tilde{\boldsymbol{B}}_l$	Modified modulator conversion losses in case of a coupling to phase shifter 1.
$\boldsymbol{H}$	Transfer function of the device under test; $\boldsymbol{H} = \alpha_{\mathrm{DUT}}\, e^{j\Psi \mathrm{DUT}}$.
$\boldsymbol{H}_R$	Weighted linear combination of all or a subset of the complex IF amplitudes V_n, $n = 1, \cdots, 8$, for an evaluation of $\boldsymbol{H}$; ideally, $\boldsymbol{H}_R = \tilde{\boldsymbol{K}}\boldsymbol{H}$; $\tilde{\boldsymbol{K}} \triangleq$ system constant.
$\boldsymbol{K}, \boldsymbol{K}_0, \tilde{\boldsymbol{K}}$	System constants.
$\boldsymbol{k}_i, i = 1,2,3$	Characteristic of binary phase shifter PSi, i.e., $\lvert\boldsymbol{k}_i\rvert \triangleq$ insertion loss change, $\arg\{\boldsymbol{k}_i\} = \Delta\Phi \triangleq$ differential phase shift.
$\boldsymbol{k}_{iu}, \boldsymbol{k}_{il}$	Characteristic of PSi for the first upper and lower sideband frequencies.
$\tilde{\boldsymbol{k}}_{1u}, \tilde{\boldsymbol{k}}_{1l}$	Modified characteristic of PS1 in case of a coupling to modulator M.
P_{RF}	Double-sideband mixer input power level.
$\boldsymbol{p}_i, i = 1,2,3$	Weighting factors for the determination of the transfer function $\boldsymbol{H}$ through $\boldsymbol{H}_R$.
$V_n, n = 1, \cdots, 8$	Complex amplitude of the IF output signal for the eight switching-state combinations of PS1, PS2, and PS3.

Auxiliary Variables

$$\tilde{\boldsymbol{B}} = \boldsymbol{B}_u + \boldsymbol{B}_l$$
$$\tilde{\boldsymbol{k}}_1 = \boldsymbol{B}_u/\tilde{\boldsymbol{B}} \cdot \boldsymbol{k}_{1u} + \boldsymbol{B}_l/\tilde{\boldsymbol{B}} \cdot \boldsymbol{k}_{1l}$$
$$\tilde{\tilde{\boldsymbol{B}}} = \boldsymbol{B}_u - \boldsymbol{B}_l$$
$$\tilde{\tilde{\boldsymbol{k}}}_1 = \boldsymbol{B}_u/\tilde{\tilde{\boldsymbol{B}}} \cdot \boldsymbol{k}_{1u} - \boldsymbol{B}_l/\tilde{\tilde{\boldsymbol{B}}} \cdot \boldsymbol{k}_{1l}$$
$$U_n = 2\,\mathrm{Re}\{V_n\}, n = 1, \cdots, 8$$
$$I_n = 2j\,\mathrm{Im}\{V_n\}, n = 1, \cdots, 8$$

Manuscript received January 27, 1986; revised March 5, 1986. This work was supported in part by the Deutsche Forschungsgemeinschaft.

The authors are with the Institut für Hoch- und Höchstfrequenztechnik, Ruhr-Universität Bochum, D-4630 Bochum, Federal Republic of Germany.

IEEE Log Number 8609060.

I. Introduction

Until now the research in homodyne systems for the determination of the complex scattering parameters of a device under test (DUT) has mainly focused on five- or six-port techniques. A traditional drawback of this type of network analyzer (NWA) is the restricted dynamic range due to a limited resolution of the power meters [1].

This paper presents an X-band NWA system based on a novel principle [2]–[4] which combines the simplicity of the RF hardware used with the potential sensitivity of heterodyne detection principles.

II. System Concept

A block diagramm of the NWA circuit is given in Fig. 1. The object connected to the test ports of the system may either be the DUT itself for transmission measurements or a test set for combined transmission/reflection measurements.

A homodyne linear downconversion of the test signal (employing, e.g., a balanced mixer) only yields the real part of its complex amplitude. However, amplitude and phase information are gained if the test signal is subjected to a digital triple-phase modulation prior to frequency conversion using three decoupled binary phase shifters PS1, PS2, PS3 [2]–[4]. An additional amplitude or phase modulation with a modulation frequency of, e.g., $f_m = 10$ kHz together with a synchronous detection in the intermediate frequency (IF) range increases the sensitivity of the system since it allows a low-noise narrow-band amplification of the IF signal for a better noise reduction.

The position of the modulator is determined by technical considerations. The backward isolation of the chain of phase shifters attenuates the LO signal leaking through the mixer which —if reflected at the modulator—yields a disturbing crosstalk.

Because of the use of three decoupled digital phase shifters, the transfer function of the series connection of PS 1,2,3 can adopt eight different values, and thus the modulated test signal is converted to an IF signal of 10 kHz with eight different and in general complex amplitudes $V_n, n = 1, \cdots, 8$.

A fast but approximate evaluation of the test signal from the measurement data is obtained—save for a complex system constant—with increasing accuracy from a weighted sum of 2, 4, or 8 of the complex amplitudes $V_n, n = 1, \cdots, 8$.

An exact solution of the system equations is time consuming and requires a minimum of three decoupled phase shifters. It yields the complex amplitude of the test signal as well as the characteristics of PS 1,2,3—which are needed for the weighted evaluation—irrespective of the amplitude and phase of the test signal. Thus, it is very useful as a calibration algorithm.

III. System Equations

Consider a test signal with a complex amplitude $\boldsymbol{K}_0 \cdot \boldsymbol{H}$ where $\boldsymbol{K}_0$ is a system constant and $\boldsymbol{H}$ is the transfer function of the DUT (including error terms for crosstalk, mismatch, etc., which have to be removed by calibration measurements). This signal is fed to a modulator M operating at $f_m = 10$ kHz with the conversion factors $\boldsymbol{B}_u$ and $\boldsymbol{B}_l$ to the first upper and lower sidebands and three cascaded and decoupled phase shifters with their respective characteristics $\boldsymbol{k}_{iu,l}, i = 1, \cdots, 3$, where the $\boldsymbol{k}_{iu,l}$ describe the phase shift and insertion loss changes of the binary elements for the upper and lower sideband frequencies.

The complex amplitude of the IF signal after a bandpass filtering with a center frequency $f_c = f_m$ is obtained as the sum of the complex RF amplitude of the upper sideband and the complex conjugate of the RF amplitude of the lower sideband.

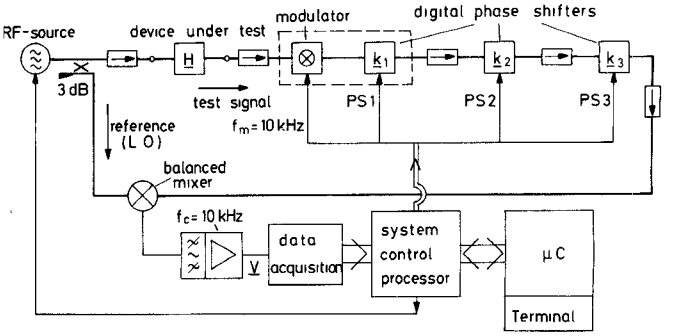

Fig. 1. Computer-controlled homodyne X-band network analyzer system.

Therefore, the following eight system equations are valid:

$$\boldsymbol{V}_1 = \boldsymbol{KHB}_u + \boldsymbol{K}^*\boldsymbol{H}^*\boldsymbol{B}_l^* \tag{1a}$$

$$\boldsymbol{V}_2 = \boldsymbol{KHB}_u\boldsymbol{k}_{1u} + \boldsymbol{K}^*\boldsymbol{H}^*\boldsymbol{B}_l^*\boldsymbol{k}_{1l}^* \tag{1b}$$

$$\boldsymbol{V}_3 = \boldsymbol{KHB}_u\boldsymbol{k}_{2u} + \boldsymbol{K}^*\boldsymbol{H}^*\boldsymbol{B}_l^*\boldsymbol{k}_{2l}^* \tag{1c}$$

$$\boldsymbol{V}_4 = \boldsymbol{KHB}_u\boldsymbol{k}_{3u} + \boldsymbol{K}^*\boldsymbol{H}^*\boldsymbol{B}_l^*\boldsymbol{k}_{3l}^* \tag{1d}$$

$$\boldsymbol{V}_5 = \boldsymbol{KHB}_u\boldsymbol{k}_{1u}\boldsymbol{k}_{2u} + \boldsymbol{K}^*\boldsymbol{H}^*\boldsymbol{B}_l^*\boldsymbol{k}_{1l}^*\boldsymbol{k}_{2l}^* \tag{1e}$$

$$\boldsymbol{V}_6 = \boldsymbol{KHB}_u\boldsymbol{k}_{1u}\boldsymbol{k}_{3u} + \boldsymbol{K}^*\boldsymbol{H}^*\boldsymbol{B}_l^*\boldsymbol{k}_{1l}^*\boldsymbol{k}_{3l}^* \tag{1f}$$

$$\boldsymbol{V}_7 = \boldsymbol{KHB}_u\boldsymbol{k}_{2u}\boldsymbol{k}_{3u} + \boldsymbol{K}^*\boldsymbol{H}^*\boldsymbol{B}_l^*\boldsymbol{k}_{2l}^*\boldsymbol{k}_{3l}^* \tag{1g}$$

$$\boldsymbol{V}_8 = \boldsymbol{KHB}_u\boldsymbol{k}_{1u}\boldsymbol{k}_{2u}\boldsymbol{k}_{3u} + \boldsymbol{K}^*\boldsymbol{H}^*\boldsymbol{B}_l^*\boldsymbol{k}_{1l}^*\boldsymbol{k}_{2l}^*\boldsymbol{k}_{3l}^*. \tag{1h}$$

A solution is sought for the complex transfer function from the set or a subset of the eight complex IF amplitudes $V_n, n = 1, \cdots, 8$, where the integer n relates to the eight possible switching state combinations of the three binary phase shifters PS 1, 2, 3.

In general, the equations (1a)–(1h) form a system of eight complex equations for the eight complex unknowns $\boldsymbol{K} \cdot \boldsymbol{H} \cdot \boldsymbol{B}_u, \boldsymbol{K}^* \cdot \boldsymbol{H}^* \cdot \boldsymbol{B}_l^*, \boldsymbol{k}_{1u}, \boldsymbol{k}_{1l}^*, \boldsymbol{k}_{2u}, \boldsymbol{k}_{2l}^*, \boldsymbol{k}_{3u}, \boldsymbol{k}_{3l}^*$ since the conversion factor $\boldsymbol{B}$ as well as the phase shifter characteristics $\boldsymbol{k}_i$ may differ for the upper and lower sideband frequencies. Obviously, it is not possible to solve (1a)–(1h) directly for $\boldsymbol{H}$. This unknown has to be determined from a solution for either $\boldsymbol{K} \cdot \boldsymbol{H} \cdot \boldsymbol{B}_u$ or $\boldsymbol{K}^* \cdot \boldsymbol{H}^* \cdot \boldsymbol{B}_l^*$. If the modulation frequency is chosen small compared to the bandwidth of the phase shifters and if a decoupled amplitude modulator with symmetrical sidebands ($\boldsymbol{B}_u = \boldsymbol{B}_l$) is employed, it is a good approximation to assume $\boldsymbol{B}_u = \boldsymbol{B}_l, \boldsymbol{k}_{iu} = \boldsymbol{k}_{il}$, whereby (1a)–(1h) degenerates to a system of eight real equations in four complex unknowns. The use of a single-sideband modulator ($\boldsymbol{B}_u \neq \boldsymbol{B}_l$) will lead to a system of eight complex equations in five complex unknowns for $\boldsymbol{k}_{iu} = \boldsymbol{k}_{il}, i = 1,2,3$.

Assuming a mutual coupling of M and PS1 the conversion factors $\boldsymbol{B}_{u,l}$ will no longer be independent of the setting of PS1, i.e.,

$$\boldsymbol{V}_1 = \boldsymbol{KHB}_u + \boldsymbol{K}^*\boldsymbol{H}^*\boldsymbol{B}_l^* \tag{2a}$$

$$\boldsymbol{V}_2 = \boldsymbol{KH}\tilde{\boldsymbol{B}}_u\tilde{\boldsymbol{k}}_{1u} + \boldsymbol{K}^*\boldsymbol{H}^*\tilde{\boldsymbol{B}}_l^*\tilde{\boldsymbol{k}}_{1l}^* \tag{2b}$$

where the tilde denotes the modification due to coupling. This can be taken into account by assuming a modification of the characteristics $\boldsymbol{k}_{1u,l}$

$$\boldsymbol{k}_{1u,l} = \tilde{\boldsymbol{B}}_{u,l}/\boldsymbol{B}_{u,l} \cdot \tilde{\boldsymbol{k}}_{1u,l}. \tag{3}$$

Then a nonlinear system similiar to (1a)–(1h) with at least six complex unknowns $\boldsymbol{K} \cdot \boldsymbol{H} \cdot \boldsymbol{B}_u$, $\boldsymbol{K}^* \cdot \boldsymbol{H}^* \cdot \boldsymbol{B}_l^*$, $\boldsymbol{k}_{1u}$, $\boldsymbol{k}_{1l}^*$, $\boldsymbol{k}_{2u} = \boldsymbol{k}_{2l} = \boldsymbol{k}_2$, $\boldsymbol{k}_{3u} = \boldsymbol{k}_{3l} = \boldsymbol{k}_3$ will result.

IV. Algebraic Solutions

A possible way for an exact and general solution to the complex system in eight complex unknowns is given in Appendix A.

Since the evaluation of the transfer function $\boldsymbol{H}$ via (A8)–(A10) involves a lot of complex algebra, it may be unsuitable for real-time applications. The computing effort may be reduced if one of the special cases (e.g., $\boldsymbol{k}_{iu} = \boldsymbol{k}_{il}$, $i = 2,3$) discussed above is encountered and if this knowledge of the unknowns is applied while solving (1a)–(1h).

It is shown in Appendix B that a system of eight complex equations with up to six complex unknowns may be solved for the complex amplitude of the test signal $\boldsymbol{KH}$ by separating the equations (1a)–(1h) into their real and imaginary parts and by solving only the real subsystem. If necessary, further information about the rest of the unknowns may be obtained by using up to four equations of the imaginary subsystem.

As a practical outcome in nearly all cases considered here, only the real part of the IF signal has to be sampled, and thus the amount of data to be handled is reduced, computation is facilitated, and thus the system speed is enhanced.

V. An Approximate Solution

For a still more rapid evaluation of the measurement data, it is advantageous to determine the test signal with the help of a different algorithm, a linear combination of two, four, or eight of the complex quantities V_n, $n = 1, \cdots, 8$ [2]. Using, e.g., only PS1 and PS2, one obtains $V_{1,2,3,5}$ and may form a linear combination

$$\begin{aligned} \boldsymbol{H}_R &= V_1 + \boldsymbol{p}_1 V_2 + \boldsymbol{p}_2 V_3 + \boldsymbol{p}_1 \boldsymbol{p}_2 V_5 \\ &= \boldsymbol{KHB}_u (1 + \boldsymbol{p}_1 \boldsymbol{k}_{1u})(1 + \boldsymbol{p}_2 \boldsymbol{k}_{2u}) \\ &\quad + \boldsymbol{K}^* \boldsymbol{H}^* \boldsymbol{B}_l^* (1 + \boldsymbol{p}_1 \boldsymbol{k}_{1l}^*)(1 + \boldsymbol{p}_2 \boldsymbol{k}_{2l}^*). \end{aligned} \tag{4}$$

It is obvious that the right choice of the $\boldsymbol{p}_i$ is given by

$$\boldsymbol{p}_i = -1/\boldsymbol{k}_{il}^* \tag{5}$$

which leaves

$$\boldsymbol{H}_R = \tilde{\boldsymbol{K}} \boldsymbol{H} \tag{6}$$

where $\tilde{\boldsymbol{K}}$ is a complex system constant. Since the error term in (6) resulting from a poor choice of the $\boldsymbol{p}_i$ is of second order, only good estimates for the $\boldsymbol{k}_{il}^*$ have to be provided.

VI. Data Acquisition and System Control

In order to acquire the complex IF amplitude V_n, $n = 1, \cdots, 8$, a syncronous modulation and sampling process is used.

Following the setting of the phase shifters, a quartz stable square wave signal of $f_m = 10$ kHz is applied to the modulator. After the decay of the transient response of the bandpass filter, the sinusoidal filter output is sampled and digitally converted each quarter of a cycle to yield the real and imaginary parts of V (the chosen settling time is 15 cycles and 3 cycles for sampling). The data acquisition unit includes a software-controlled prescaler amplifier to enhance the dynamic range of the system.

The network analyzer setup is linked to a microcomputer system (μC) by a special subprocessor unit (Fig. 2) which is devoted to control frequency, RF phase shift, modulation, and data acquisition with automatic gain control.

The measurement values are stored in a 2 kbyte data buffer. After completion of one data acquisition cycle, the microcomputer gains access to the data storage area using bus multiplexers.

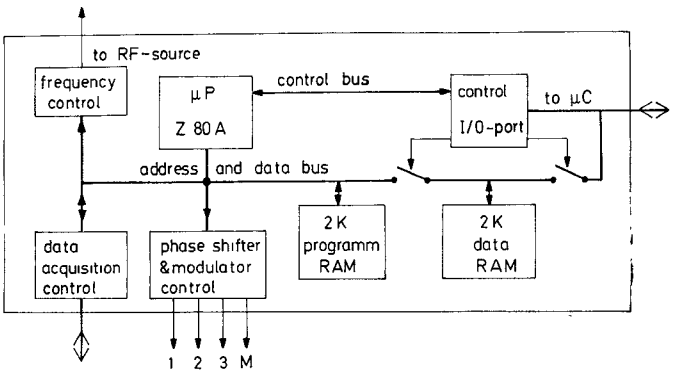

Fig. 2. Subprocessor for automated data acquisition and system control.

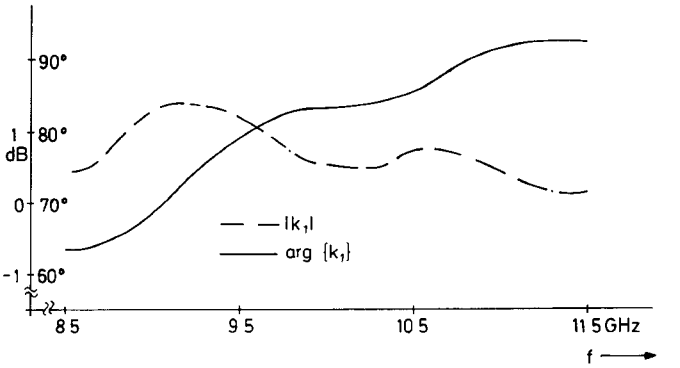

Fig. 3. Characteristic $\boldsymbol{k}_1$ of pin-diode "switched-line" phase shifter PS1; $\arg\{\boldsymbol{k}_1\}$ = differential phase shift; $|\boldsymbol{k}_1|$ = insertion loss change; obtained via the algebraic solution (A8).

VII. Data Processing and Measurements Results

For an increased system speed, only PS1 and PS2 are used together with a weighted evaluation of the measurement data $V_{1,2,3,5}$ (see Section V). As a prerequisite, estimates for the characteristics $\boldsymbol{k}_{1l}, \boldsymbol{k}_{2l}$ have to be available. These are provided by a single measurement cycle over the frequency range employing three phase shifters and the algebraic solution for $\boldsymbol{k}_{1l}^*, \boldsymbol{k}_{2l}^*$ of (A8) and (A5). They are stored together with possible additional calibration terms derived from error correction measurements.

The characteristic $\boldsymbol{k}_1$ of PS1 (decoupled pin-diode "switched line" phase shifter, $\boldsymbol{k}_{iu} = \boldsymbol{k}_{il}$) is shown in Fig. 3 for 32 discrete frequencies in the range of 8.5–11.5 GHz as given by the exact solution of (A8).

To check the broad-band measuring capabilities of this system, the transfer phase of a precision waveguide phase shifter (HP X 855A) has been measured in the range of 8.5–11.5 GHz for the settings of the DUT of 0, 45, 90°, $\cdots$. The maximum deviation of the calculated values from the reading of the DUT were limited to $+/-3°$ over the whole frequency range, but this includes the nonideality of the reference phase shifter.

The dynamic range of the system is demonstrated by Fig. 4. The DUT has been realized by a series connection of two waveguide attenuators and a precision waveguide phase shifter. Phase linearity errors are limited to approximately $+/-0.8°$ for a double-sideband mixer input power level (P_{RF}) of -20 dBm up to $+/-3°$ for $P_{RF} = -80$ dBm.

It is interesting to note that Fig. 4(a) and (b) compares well with typical phase error curves for commercial rotary vane phase shifters as given, e.g., in [6], which show a strong "second harmonic" component. From this, it may be concluded that the systematic phase detection errors which stem from a nonideal

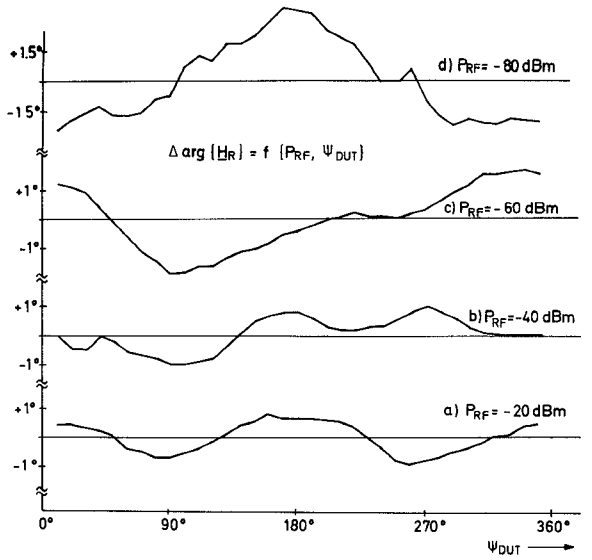

Fig. 4. Deviations of the calculated phase arg $\{H_R\}$ from linearity versus the transfer phase Ψ_{DUT} of a calibrated rotary vane phase shifter for a double-sideband mixer input power level of -20 to -80 dBm, $f = 10$ GHz.

vector–voltmeter operation of the triple-stage phase shifter configuration are at least below $\pm 0.5°$. For lower power levels, the phase error increases and displays a significant "first harmonic" error component, which is typical for crosstalk interference. Such errors may be reduced by system error correction procedures, but should be minimized in advance by an improved system design, like better grounding, shielding, and backward isolation.

Some efforts have yet to be made to improve the signal-to-noise ratio, which at present is limited by the interference of the computer clock pulse. A substantial improvement is expected if a refined IF circuitry is used.

VIII. Accuracy Limits Due to Systematic Errors

The nonideal behavior of the network analyzer circuit due to test-port mismatch, directivity, and crosstalk can be minimized by standard means if the vector voltmeter operation of the circuit itself is exact. The latter is mainly influenced by the coupling of two neighboring phase shifters used.

The only important interaction of the phase shifters stems from a switching-state-dependent reflection coefficient $\Gamma_{01} +/- \Delta\Gamma, \Gamma_{i2} +/- \Delta\Gamma$ of the output port of, e.g., PS1, and the input port of PS2 if the phase shifters are operated between a matched source and a matched load.

A numerical example shows that a $|\Delta\Gamma|$ of -20 dB together with an isolation of 20 dB will yield worst case phase and amplitude errors of 0.06° and 0.009 dB, respectively.

Measurement errors due to poor weighting factors are within the same limits if $\arg\{k_1\}, |k_1|$ are known within an error limit of $+/-5°$ and 0.5 dB, respectively. This is absolutely assured if they are provided by the exact solution of (A8).

IX. Conclusions

The homodyne network analyzer system reported exhibits broad-band measuring capabilities as well as a high sensitivity. Phase detection errors are limited to $+/-0.8°$ for a mixer input level of -20 dBm with an increase up to $+/-3°$ for a mixer level of -80 dBm and should be improvable. On account of its simple RF structure the system may serve as a model for a millimeter wave network analyzer to be developed.

Appendix A

A short outline of a general algebraic solution of the system (1a)–(1h) of eight complex equations in eight complex unknowns $\boldsymbol{K}\cdot\boldsymbol{H}\cdot\boldsymbol{B}_u, \boldsymbol{K}^*\cdot\boldsymbol{H}^*\cdot\boldsymbol{B}_l^*, k_{1u}, k_{1l}^*, k_{2u}, k_{2l}^*, k_{3u}, k_{3l}^*$ shall be given here.

Multiplying (1a) with k_{1l}^* and subtracting it from (1b) yields

$$V_2 - V_1 k_{1l}^* = \boldsymbol{KHB}_u(k_{1u} - k_{1l}^*). \tag{A1}$$

Applying the same procedure to (1c) and (1e), (1d) and (1f), (1g) and (1h), one obtains

$$V_5 - V_3 k_{1l}^* = \boldsymbol{KHB}_u k_{2u}(k_{1u} - k_{1l}^*) \tag{A2}$$

$$V_6 - V_4 k_{1l}^* = \boldsymbol{KHB}_u k_{3u}(k_{1u} - k_{1l}^*) \tag{A3}$$

$$V_8 - V_7 k_{1l}^* = \boldsymbol{KHB}_u k_{2u} k_{3u}(k_{1u} - k_{1l}^*). \tag{A4}$$

Dividing (A2) as well as (A3) and (A4) by (A1), we gain three functional relations

$$k_{2u} = f_2\{k_{1l}^*\}; \qquad k_{3u} = f_3\{k_{1l}^*\}; \qquad k_{2u}\cdot k_{3u} = f_{23}\{k_{1l}^*\}$$

with

$$k_{2u} = f_2\{k_{1l}^*\} = (V_5 - V_3 k_{1l}^*)/(V_2 - V_1 k_{1l}^*) \tag{A5}$$

$$k_{3u} = f_3\{k_{1l}^*\} = (V_6 - V_4 k_{1l}^*)/(V_2 - V_1 k_{1l}^*) \tag{A6}$$

$$k_{2u}\cdot k_{3u} = f_{23}\{k_{1l}^*\} = (V_8 - V_7 k_{1l}^*)/(V_2 - V_1 k_{1l}^*). \tag{A7}$$

Therefore, one may solve a quadratic equation in k_{1l}^*

$$f_2\{k_{1l}^*\}\cdot f_3\{k_{1l}^*\} = f_{23}\{k_{1l}^*\}$$

which results in the solution

$$k_{1l}^* = u +/- j\cdot w \tag{A8}$$

with

$$u = \frac{b}{2a} \qquad w = \frac{\sqrt{4ac - b^2}}{2a}$$

and

$$a = V_{34} - V_{17}; \qquad b = V_{45} + V_{36} - V_{18} - V_{27}$$

$$c = V_{56} - V_{28}; \qquad V_{mn} = V_m\cdot V_n; \qquad m, n = 1, \cdots, 8.$$

Exactly the same solution is obtained for k_{1u} if (1a), (1c), (1d), (1g) are multiplied by k_{1u} instead of k_{1l} and if the same procedure as outlined above is followed. It is seen that both unknowns k_{1u}, k_{1l}^* only differ by the sign of the root in (A8). For the special case of $k_{1u} = k_{1l}$ it may be shown that u as well as w are real quantities, and therefore $k_1^* = u +/- jw$ and $k_1 = u -/+ jw$, as is to be expected. The ambiguity of the sign still has to be resolved by some information about, e.g., k_1, for instance, whether the phase change of PS1 is positive or negative. The same derivation holds if $V_1 \cdots V_8$ are real [4, eqs. 2,7–10].

The phase shifter characteristics k_{2u}, k_{3u} are now obtained via (A5) and (A6), whereas k_{2l}^* and k_{3l}^* are gained from (A5) and (A6) by replacing k_{1l}^* by k_{1u}.

Finally, with the help of (A8), the complex amplitude of the test signal is obtained from (1a) and (1b)

$$\boldsymbol{KHB}_u = \frac{1}{2}\cdot(V_1 +/- j(V_2 - uV_1)/w) \tag{A9}$$

or

$$\boldsymbol{K}^*\boldsymbol{H}^*\boldsymbol{B}_l^* = \frac{1}{2}\cdot(V_1 -/+ j(V_2 - uV_1)/w). \tag{A10}$$

The unknown system constants $\boldsymbol{K}\cdot\boldsymbol{B}_u, \boldsymbol{K}\cdot\boldsymbol{B}_l$ are determined by replacing the DUT by a known through connection or—for high precision measurements—using calibration standards for vector error correction procedures [5].

APPENDIX B

It will be shown that—under certain circumstances—the complex amplitude of the test signal may be obtained analytically by using only the real part of the complex amplitude of the IF signal

$$U_n = 2 \cdot \mathrm{Re}\{V_n\} = V_n + V_n^*, \qquad n = 1, \cdots, 8 \tag{B1}$$

where the IF amplitudes V_n are given by (1a)–(1h). For this purpose, the characteristic of at least two phase shifters must meet the requirement that its value is equal for the upper and lower sideband frequencies. The special case $k_{2u} = k_{2l} = k_2$, $k_{3u} = k_{3l} = k_3$, and $B_u \neq B_l, k_{1u} \neq k_{1l}$ shall be considered here as an example.

With the help of (B1), one obtains U_1 from (1a)

$$U_1 = K \cdot H \cdot (B_u + B_l) + K^* \cdot H^* \cdot (B_u + B_l)^* \tag{B2}$$

and in a similar fashion one obtains U_2 from (1b) via (B1)

$$\begin{aligned} U_2 = {} & KH(B_u + B_l)\left[B_u/(B_u + B_l) \cdot k_{1u} + B_l/(B_u + B_l) \cdot k_{1l}\right] \\ & + K^*H^*(B_u + B_l)^* \\ & \cdot \left[B_u/(B_u + B_l) \cdot k_{1u} + B_l/(B_u + B_l) \cdot k_{1l}\right]^*. \end{aligned} \tag{B3}$$

The rest of the real parts U_3–U_8 may be written in analogy to (B2), and (B3), and one arrives at a system of eight real equations in four complex unknowns

$$U_1 = KH\tilde{B} + K^*H^*\tilde{B}^* \tag{B4a}$$

$$U_2 = KH\tilde{B}\tilde{k}_1 + K^*H^*\tilde{B}^*\tilde{k}_1^* \tag{B4b}$$

$$U_3 = KH\tilde{B}k_2 + K^*H^*B^*k_2^* \tag{B4c}$$

$$U_4 = KH\tilde{B}k_3 + K^*H^*\tilde{B}^*k_3^* \tag{B4d}$$

$$U_5 = KH\tilde{B}\tilde{k}_1k_2 + K^*H^*\tilde{B}^*\tilde{k}_1^*k_2^* \tag{B4e}$$

$$U_6 = KH\tilde{B}\tilde{k}_1k_3 + K^*H^*\tilde{B}^*\tilde{k}_1^*k_3^* \tag{B4f}$$

$$U_7 = KH\tilde{B}k_2k_3 + K^*H^*\tilde{B}^*k_2^*k_3^* \tag{B4g}$$

$$U_8 = KH\tilde{B}\tilde{k}_1k_2k_3 + K^*H^*\tilde{B}^*\tilde{k}_1^*k_2^*k_3^* \tag{B4h}$$

where the abbreviations

$$\tilde{B} = B_u + B_l \tag{B5}$$

and

$$\tilde{k}_1 = B_u/\tilde{B} \cdot k_{1u} + B_l/\tilde{B} \cdot k_{1l} \tag{B6}$$

have been used. This notation includes the special cases $\tilde{k}_1 = k_1$ for $k_{1u} = k_{1l} = k_1$ and $\tilde{B} = 2B$ for $B_u = B_l = B$.

It is seen that the system (B4a)–(B4h) is structurally identical to (1a)–(1h), and a solution for the unknowns $KH\tilde{B}, \tilde{k}_1, k_2, k_3$ is readily obtained from (A9), (A8), (A5), (A6) by replacing V_i by U_i, KHB_u by $KH\tilde{B}$, k_{1u} by $\tilde{k}_1$, and $k_{2,3u}$ by $k_{2,3}$.

The solution to the real subsystem thus yields the complex transfer function of the DUT multiplied by the average of the modulator conversion factors B_u and B_l and a complex system constant K. Both unknown constants have to be removed by one calibration measurement (cf. Appendix A). Furthermore, a weighted average of the phase shifter characteristic $k_{1u,l}$ for the upper and lower sideband frequency is obtained. The solutions for $k_{2,3}$ are exact.

For certain applications a separate determination of $K \cdot H \cdot B_u$, $K \cdot H \cdot B_l$, as well as k_{1u} and k_{1l}, may be desirable. This may be accomplished by using additional information from the imaginary subsystem of (1a)–(1h).

We define

$$I_n = 2 \cdot j \cdot \mathrm{Im}\{V_n\} = V_n - V_n^* \tag{B7}$$

and obtain from (1a)

$$I_1 = KH\tilde{\tilde{B}} - K^*H^*\tilde{\tilde{B}}^* \tag{B8}$$

with

$$\tilde{\tilde{B}} = B_u - B_l \tag{B9}$$

and from (1c)

$$I_3 = KH\tilde{\tilde{B}}k_2 - K^*H^*\tilde{\tilde{B}}^*k_2^*. \tag{B10}$$

We may now solve (B8) and (B10) for $KH\tilde{\tilde{B}}$

$$KH\tilde{\tilde{B}} = (I_3 - k_2^* \cdot I_1)/(k_2 - k_2^*). \tag{B11}$$

With $KH(B_u + B_l)$ and k_2 given by the solution to the real subsystem and $KH(B_u - B_l)$ given by (B11), KHB_u as well as KHB_l are known.

In order to solve for $k_{1u,l}$, we may write the imaginary part of V_2 as

$$I_2 = KH\tilde{\tilde{B}}\tilde{\tilde{k}}_1 - K^*H^*\tilde{\tilde{B}}^*\tilde{\tilde{k}}_1^* \tag{B12}$$

with $\tilde{\tilde{B}}$ defined by (B9) and

$$\tilde{\tilde{k}}_1 = B_u/\tilde{\tilde{B}} \cdot k_{1u} - B_l/\tilde{\tilde{B}} \cdot k_{1l}. \tag{B13}$$

Similarly, we obtain I_5

$$I_5 = KH\tilde{\tilde{B}}\tilde{\tilde{k}}_1k_2 - K^*H^*\tilde{\tilde{B}}^*\tilde{\tilde{k}}_1^*k_2^* \tag{B14}$$

and solve (B12) and (B14) for $\tilde{\tilde{k}}_1$

$$\tilde{\tilde{k}}_1 = (I_5 - k_2^*I_2)/K \cdot H \cdot \tilde{\tilde{B}} \cdot (k_2 - k_2^*). \tag{B15}$$

Finally, we obtain $k_{1u,l}$ from (B6) and (B13)

$$k_{1u} = 1/2 \cdot \left((B_u + B_l)/B_u \cdot \tilde{k}_1 + (B_u - B_l)/B_u \cdot \tilde{\tilde{k}}_1\right) \tag{B16}$$

$$k_{1l} = 1/2 \cdot \left((B_u + B_l)/B_l \cdot \tilde{k}_1 - (B_u - B_l)/B_l \cdot \tilde{\tilde{k}}_1\right) \tag{B17}$$

whereby all unknowns are determined.

It may easily be shown that all results given above may be obtained irrespectively of the transfer phase of the IF circuitry or any constant time offset in the sampling process. Nevertheless—for practical purposes–it is advantageous to choose the fixed point of time for the sampling of the real part near the maximum of the IF signal for an improved signal-to-noise ratio.

ACKNOWLEDGMENT

The authors wish to acknowledge the financial support of the Deutsche Forschungsgemeinschaft. They appreciate the continuing scientific support of H. Severin and R. Frese and the contributions of R. Pawellek, J. Ney, H. Osterwinter, A. Baumeister, H. Geppert, and P. Piankowsky, who developed and improved the system hardware and software.

REFERENCES

[1] C. A. Hoer, "Performance of a dual six-port automatic network analyser," *IEEE Trans. Microwave Theory Tech.*, vol. MTT-27, pp. 993–998, Dec. 1979.

[2] U. Gärtner and B. Schiek, "Homodyne network analysis by digital phase modulation and baseband sampling," *Electron. Lett.*, vol. 20, no. 2, pp. 73–75, Jan. 1984.

[3] ———, "Homodyne network analysis by a digital triple phase modulation and baseband sampling technique," in *Conf. Dig. CPEM 1984*, Delft, The Netherlands, pp. 134–136.

[4] ———, "An automatic homodyne network analyser with phase shift keying and baseband sampling," in *Proc. 14th EuMC 1984*, pp. 813–818.

[5] "Automating the HP 8410B microwave network analyser," Appl Note 221A, Hewlett-Packard, June 1980.

[6] P. I. Somlo, D. L. Hollway, and I. G. Morgan, "The absolute calibration of periodic microwave phase shifters without a standard phase shifter," *IEEE Trans. Microwave Theory Tech.*, vol. MTT-20, pp. 532–537, Aug. 1972.